ENVIRONMENTAL RESEARCH
LETTERS

LETTER • OPEN ACCESS

West-warming East-cooling trend over Antarctica reversed since early 21st century driven by large-scale circulation variation

ENVIRONMENTAL RESEARCH
LETTERS

LETTER

West-warming East-cooling trend over Antarctica reversed since early 21st century driven by large-scale circulation variation

Meijiao Xin[1,2], **Kyle R Clem**[3], **John Turner**[4], **Sharon E Stammerjohn**[5], **Jiang Zhu**[1], **Wenju Cai**[6,7] and **Xichen Li**[1,*]

[1] Institute of Atmospheric Physics, Chinese Academy of Sciences, Beijing 100029, People's Republic of China
[2] College of Earth and Planetary Sciences, University of Chinese Academy of Sciences, Beijing 100049, People's Republic of China
[3] School of Geography, Environment and Earth Sciences, Victoria University of Wellington, 6012 Wellington, New Zealand
[4] British Antarctic Survey, Natural Environment Research Council, Cambridge CB30ET, United Kingdom
[5] Institute of Arctic and Alpine Research, University of Colorado, Boulder, CO 80309, United States of America
[6] Key Laboratory of Physical Oceanography/Institute for Advanced Ocean Studies, Ocean University of China and Qingdao National Laboratory for Marine Science and Technology, Qingdao 266003, People's Republic of China
[7] Centre for Southern Hemisphere Oceans Research (CSHOR), CSIRO Oceans and Atmosphere, Hobart, Tasmania 7004, Australia
* Author to whom any correspondence should be addressed.

E-mail: lixichen@mail.iap.ac.cn

Keywords: Antarctic rapid warming, seesaw temperature pattern, thermal advection

Supplementary material for this article is available online

OPEN ACCESS

RECEIVED
8 February 2023

REVISED
5 May 2023

ACCEPTED FOR PUBLICATION
25 May 2023

PUBLISHED
2 June 2023

Abstract

Antarctic climate changes prior to 2000 were characterized by a strong zonally asymmetric pattern. Over 90% of the land ice mass loss occurred around a limited area in West Antarctica, accompanied by a rapid surface warming rate about three times the global mean. In contrast, surface warming and glacier mass loss around East Antarctica are not significant, until the decades since 2000 when several individual stations show that the temperature trends might have reversed. The asymmetric climate changes between East- and West-Antarctica are largely attributable to the inter-decadal variabilities over the Pacific and Atlantic Oceans through tropical–polar teleconnections, leaving open the question of whether the post-2000 phase shift of the lower-latitude decadal variability causes a flip of the asymmetric Antarctic changes. Here, by synthesizing 26 *in-situ* observations and 6 reanalysis datasets using a statistical method and integrating the results with a series of climate model experiments, we find that the West-warming, East-cooling trend over Antarctica has systematically reversed in austral spring since the early 21st century, largely due to the atmospheric circulation anomaly over the Antarctic Peninsula–Weddell Sea region, which is associated to the teleconnection with Pacific and atmospheric internal variability. This reversal of the temperature seesaw suggests that substantial decadal-scale fluctuations of the Antarctic climate system exist, including for sea-ice and land-ice systems, superimposed on and modifying longer term changes.

1. Introduction

In the satellite era since 1979, zonally asymmetric climate changes have been observed over the Antarctic continent, the most dramatic being a rapid warming over West Antarctica and the Antarctic Peninsula [1–3], accompanied by accelerated land ice mass loss and sea ice melting [4–6]. In contrast, a mild cooling trend was observed over the East Antarctic [3, 7] accompanied by even glacial mass gain [4]. Even though the current mass loss of Antarctic ice shelves is mainly attributed to their basal melting [8], the Antarctic surface warming plays an important role in promoting the Antarctic surface mass loss in the future [9]. These seesaw-like climate changes between the East and West Antarctic have broad implications for global sea level rise [10], the global energy balance [11], and the global carbon cycle [12].

While the overall changes in Antarctic climate are driven primarily by the combined effects of anthropogenic greenhouse gas forcing [13–15] and atmospheric internal modes [16, 17], the seesaw-like

changes between East and West Antarctica have been largely attributed to atmospheric circulation changes [16, 18–20] driven by teleconnections to the tropical oceans [18–24]. The Southern Annular Mode (SAM), two Pacific South American (PSA) modes (PSA1 and PSA2) [25], and a zonal wave number three (ZW3) pattern [26, 27] contribute to the Antarctic seesaw-like climate changes, mainly through thermal advection [28–30] and its associated ocean–atmosphere–sea ice feedbacks [30, 31] and cloud feedbacks [32]. The multi-decadal changes in these atmospheric circulation patterns are linked to tropical sea surface temperature (SST) variability [18, 19, 21–23], in particular the Interdecadal Pacific Oscillation (IPO) [33, 34] and the Atlantic Multidecadal Oscillation (AMO) [20, 22, 23], through tropical–polar teleconnections [18, 19, 21–23].

Since the early 2000s, the warming trend over the North Atlantic slowed down, implying an upcoming reversal of the AMO [19], while the phase of the IPO started to switch after the 2015–2016 El Nino event [19, 33, 35]. Meanwhile, scattered observations over both the East- and the West-Antarctic reported some reversed surface air temperature (SAT) trend signals [7, 16, 36]: warming trends at several stations in West Antarctica [36] and the Antarctic Peninsula [7, 16] decreased beginning around 2000, whereas a record warming has recently been reported at the South Pole [37, 38], although with strong regional and seasonal features [7, 16, 36, 37] and a large uncertainty [1, 7, 36, 37]. This naturally raises questions as to whether a systematic adjustment of the Antarctic climate system started after 2000 and whether changes in decadal-scale tropical variability is contributing to this polar adjustment. Answering these questions requires accurate high-resolution observations for identifying the regionality, seasonality, and decadal variation in Antarctic SAT trends. Unfortunately, reliable observations for explaining this complexity are limited. Surface temperature observations from only about 20 Antarctic stations are available for assessing multi-decadal trends [7], with spatial coverage that is too sparse to represent the entire continent. Further, pronounced biases and spurious trends exist in the satellite observations [39] and reanalysis datasets over Antarctica [40, 41]. These disadvantages in existing datasets [39–41] hinder the assessment of the extent to which the inferred climate change reversals are robust or systematic and what broader processes underpin the switch.

Nevertheless, while any individual dataset may not represent the complexity of the Antarctic SAT trend, each of the above mentioned datasets provides additional information to reduce the uncertainty, underscoring the need for advanced statistical techniques that combine all available data to obtain more definitive estimates of Antarctic SAT trends. Here, using such an approach, referred to as combined maximum covariance analysis (CMCA) [42], the most coherent signals among different reanalyses and observation datasets are retrieved. We thus extract these coherent SAT modes among 26 surface stations and 6 reanalysis datasets, demonstrating that trends in East Antarctica cooling and West Antarctic warming in austral spring systematically reversed after 2000. This switch is further attributed to the large-scale adjustment of the atmospheric circulation associated with the tropical–polar teleconnection and atmospheric internal variability.

2. Materials and methods

2.1. Data

We use observed monthly SAT data from 26 Antarctic stations (see supplementary table 1) collected by the Scientific Committee on Antarctic Research Reference Antarctic Data for Environmental Research project [43]. Monthly SAT observation data for the Byrd Station is obtained from a reconstructed temperature record [2].

We also use monthly SAT and sea level pressure (SLP) data from six reanalysis datasets: (1) the Climate Forecast System Reanalysis (CFSR) [44] and the National Center for Environmental Prediction (NCEP) coupled forecast system model version 2 (CFSv2) [45]; (2) the NCEP- Department of Energy (DOE) Reanalysis version-2 (NCEP2) [46]; (3) the Modern Era Retrospective-Analysis for Research and Applications, version 2 (MERRA2) [47]; (4) the Japanese 55 year Reanalysis (JRA55) [48]; (5) the Interim reanalysis data from the European Centre for Medium-Range Weather Forecasts (ERA-Interim) [49]; and (6) the European Centre for Medium-Range Weather Forecasts Reanalysis version 5 (ERA5) [50]. Because the resolutions of these datasets differ, we interpolated all reanalysis datasets into a $2^\circ \times 2^\circ$ grid. These datasets cover a common period from 1979 to 2019, except that MERRA2 started in 1980 and ERA-Interim ended in August 2019. The monthly 500 hPa geopotential height (GPH) data from ERA5 are also used to calculate the SAM, PSA1, and PSA2 patterns and the associated time series, given the superior quality of this dataset over the Southern Hemisphere compared with other reanalysis datasets [51, 52]. In addition, the monthly Hadley Centre SST dataset (HadISST) [53] at $1^\circ \times 1^\circ$ horizontal resolution has been used to obtain the SST regression map onto time series for each mode of the CMCA (see below).

The ZW3 pattern is identified using the third harmonic of a Fourier transform of ERA5 500 hPa GPH over 1979–2019 averaged across the latitude band of 55–63°S.

2.2. The CMCA method

The CMCA method [42] is an effective statistical tool to extract the most coherent spatial-temporal modes among multiple different datasets with different mappings for the same variable [54]. Here we perform

the CMCA method on the detrended monthly SAT anomalies of the seven observational and reanalysis datasets over the Antarctic (90°S–55°S) to obtain the most prominent coherent modes of SAT interannual and decadal variability during the period of 1979–2019.

The coherent modes with the largest agreement among different datasets are calculated by maximizing the combined covariance matrix among different datasets, which is defined as:

$$\mathbf{C} = \frac{1}{q-1} \boldsymbol{X}^{\mathbf{rea}} \boldsymbol{X}^{\mathbf{obs}^{\mathrm{T}}} \quad (1)$$

where q is the sample size of each dataset, which refers to the time range. $\boldsymbol{X}^{\mathbf{obs}}$ is the state variable (SAT) of all *in-situ* observations with 26 stations, each with 123 samples for September–October–November (SON), from 1979 to 2019. $\boldsymbol{X}^{\mathbf{rea}}$ is a $6m \times q$ matrix (m is the total number of spatial grids of each reanalysis, while q is the total number of time steps), which combines the state variable of all six reanalyses at each time step.

The singular value decomposition is then performed on the combined covariance matrix **C** to retrieve the largest coherent spatial-temporal modes that maximize the cross-covariance among all reanalyses and station observations. Notably, the spatial patterns of these CMCA modes among the six reanalysis datasets show high consistency [54]. Therefore, here we use the ensemble mean of reanalyses to represent a combined reanalysis spatial pattern for each mode.

2.3. Other statistical methods

The SAM, PSA1, and PSA2 modes in this study are the first three Empirical Orthogonal Function (EOFs) [55], respectively, retrieved from the monthly ERA5 500 hPa GPH anomalies over the Southern Hemisphere (0°–90°S). Spatial correlation coefficients (weighted by the area of each grid cell) have been used to illustrate the coherence between circulation patterns associated with CMCA Mode 1 and PSA2. We use the Sen's slope method [56] to calculate the linear trend, with the significance level calculated through the Mann–Kendall test [57]. Linear regression, Pearson's correlation, and composite analysis are also used in this study to (respectively) investigate the regression maps of the CMCA time series and the correlation between PSA2 and ZW3. The statistical significance is calculated using the Student's t-test, which is undertaken using the effective degree of freedom taking the autocorrelation of the variables into consideration.

In this study, two statistical methods were employed to identify the change points of the time series. The first method utilized was the robust change point detection method developed by Alin *et al* [58]. This method identifies the robust change points by calculating the sum of squares for error for various regression models. The second method employed was the traditional moving t-test [59], which is based on the 15 year moving trend of the time series. This method detects significant change points by testing whether the trend has undergone a sudden change at a certain point. The change points are determined according to the intersection of these two methods.

3. Results

3.1. Seesaw SAT trends between East and West Antarctica

We calculate the trends of the Antarctic SAT using 26 frequently-used stations for two periods, 1979–2000 and 2001–2019. Although the sparse distribution of these stations may not represent the SAT trends over the entire Antarctic, the distribution of these warming and cooling signals depicts a seesaw-like pattern, especially for austral spring (SON). Most of the stations over West Antarctica experienced rapid warming trends before 2000 (figure 1(a)), followed by cooling trends after (figure 1(b)). This reversal is especially evident at the Faraday/Vernadsky (figure 1(c)) and Rothera (figure 1(d)) stations located at the west coast of the Antarctic Peninsula, as well as the Byrd Station (figure 1(e)) over in-land West Antarctica. In contrast, most of the stations over East Antarctica show mild, insignificant cooling trends before 2000 (figure 1(a)), followed by warming trends after (figure 1(b)). This switch is clear at the Neumayer Station (figure 1(f)) over Queen Maud Land and the Amundsen–Scott and Vostok stations (figures 1(g) and (h)) in the interior of East Antarctica.

The multi-decadal SAT trends (based on *in-situ* observations) for the other three seasons are illustrated in supplementary figure 1. Similar seesaw-like SAT trends are seen in most of these seasons, especially for austral summer (December-January-February, DJF, see supplementary figures 1(a) and (d)). However, these seesaw signals are either weaker (see supplementary figures 1(a) and (d)), or more complex (see supplementary figures 1(b), (c), (e) and (f)) than those of the austral spring (figure 1). Below we focus exclusively on the seesaw-SAT trend and its reversal in spring (SON).

To further evaluate the spatial distribution of this seesaw-like SAT trend, we illustrate the spring SAT trends before and after 2000 based on three state-of-the-art reanalysis products, namely the MERRA2 (see supplementary figures 2(a) and (d)), the JRA55 (see supplementary figures 2(b) and (e)), and the ERA5 datasets (see supplementary figures 2(c) and (f)). Although these reanalyses show some degree of the West warming-East cooling trend reversal after 2000, there is considerable discrepancy in the spatial extent and magnitude of the west–east trend pattern, which is not surprising given previously reported discrepancies among these reanalyses [40, 41]. These discrepancies hinder the further assessment of

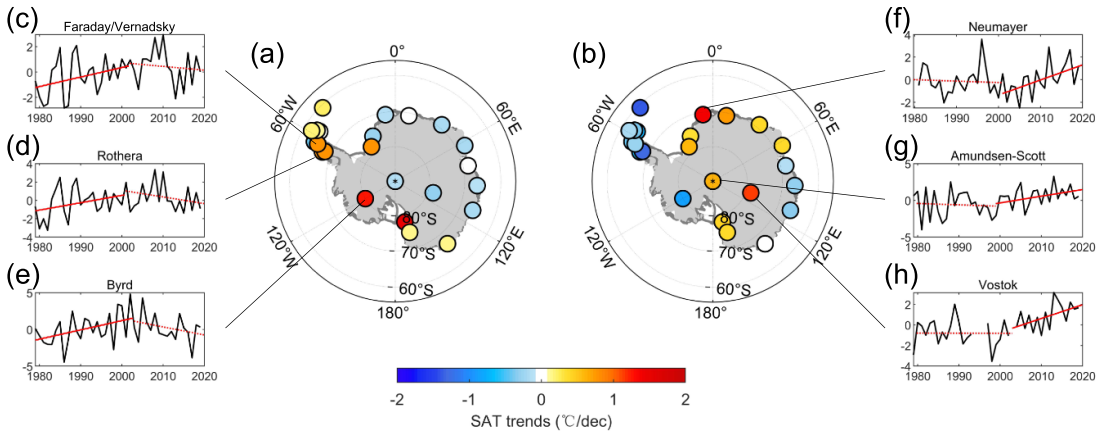

Figure 1. Austral spring (September–October–November, SON) surface air temperature (SAT) trends based on *in-situ* observations ((a) and (b)). Colored circles indicate the SON SAT trends (°C/decade) from *in-situ* observations for the periods 1979–2000 (a) and 2001–2019 (b), respectively. (c)–(h) show the SON seasonal mean time series for Faraday/Vernadsky (c), Rothera (d), Byrd (e), Neumayer (f), Amundsen–Scott (g), and Vostok (h) stations. The solid (dashed) red lines in (c)–(h) show the significant (insignificant) linear trends of the SAT at each station at $p < 0.1$. The change points in (c)–(h) are determined using the Alin's method and the moving *t*-test based on 10 year moving trend.

the west–east pattern, including its robustness or its potential causes, and call for a statistical approach that might yet distill a robust and common signal from these datasets.

Despite limited station observations and significant discrepancies between reanalysis datasets, effective methods can be used to combine all available information and extract reliable patterns of SAT variability. The CMCA method has been demonstrated to be particularly effective for this purpose, providing a means to extract coherent information from multiple datasets pertaining to the same variable [54]. In this study, we therefore apply the CMCA method to 6 reanalysis datasets and 26 *in-situ* observations to identify the most consistent modes of Antarctic SAT variability, and further investigate the robustness and underlying mechanisms of the reversal of the Antarctic SAT trend in SON.

Figure 2 shows the spatial patterns and time series of the first three CMCA modes of SON SAT. The first mode (figure 2(a)) explains 39% of the total covariance, showing a seesaw pattern between West Antarctica (including the Antarctic Peninsula) and a large portion of East Antarctica comprising Queen Maud Land and interior East Antarctica, hereafter referred to as the Antarctic-seesaw SAT pattern. Importantly, the associated time series (figure 2(b)) of Mode 1 shows a significant trend reversal in ∼2000. A significant negative trend before 2000 is observed, which represents substantial warming over West Antarctica and cooling over the Queen Maud Land area. After 2000, a significant positive trend is observed, with warming over most regions of East Antarctica and cooling over West Antarctica. In short, the first mode represents a seesaw multi-decadal SAT trend pattern between West Antarctica and the Queen Maud Land area with a phase reversal in the early 21st century.

The spatial pattern of CMCA Mode 2 (figure 2(c)) shows a pan-Antarctic cooling at its positive phase (hereafter named as Antarctic-continental SAT pattern), which might be related to the variability of the SAM [60] or radiative forcing associated with changes in greenhouse gas concentrations. Mode 3 (figure 2(e)) depicts a West Antarctic SAT-dipole pattern [61–63] between the Antarctic Peninsula and the west of Marie Byrd Land [63]. Unlike Mode 1, the time series of Modes 2 and 3 (figures 2(d) and (f)) show no significant trends. The first three modes of CMCA explain more than 86% of the covariance between the set of 26 stations and the 6 reanalysis datasets, indicating that these three modes represent the majority of SAT variability over the Antarctic in austral spring.

We also conducted a CMCA analysis on monthly temperature anomalies for the other three seasons (see supplementary figures 3 and 4). The first three leading modes show very similar spatial patterns to those for the spring, with the rank of percentage variance explained by Mode 1 (Antarctic-seesaw pattern) and Mode 2 (Antarctic-continental pattern) switched. The similarity of the leading three modes among different seasons reinforces the robustness of these dominant modes of Antarctic SAT variability. Below we discuss the circulation associated with the SON seesaw-SAT trend and its reversal.

3.2. Anomalous atmospheric circulation associated with the seesaw SAT trends

The SLP projected onto the time series of the Antarctic-seesaw SAT pattern (CMCA Mode 1) through linear regression (figure 3(a)) shows a Rossby wave-like pattern, with an anomalous high-pressure center over the Ross Sea and a low-pressure center over the Antarctic Peninsula–Weddell Sea region; the latter extends to inland Antarctica and induces

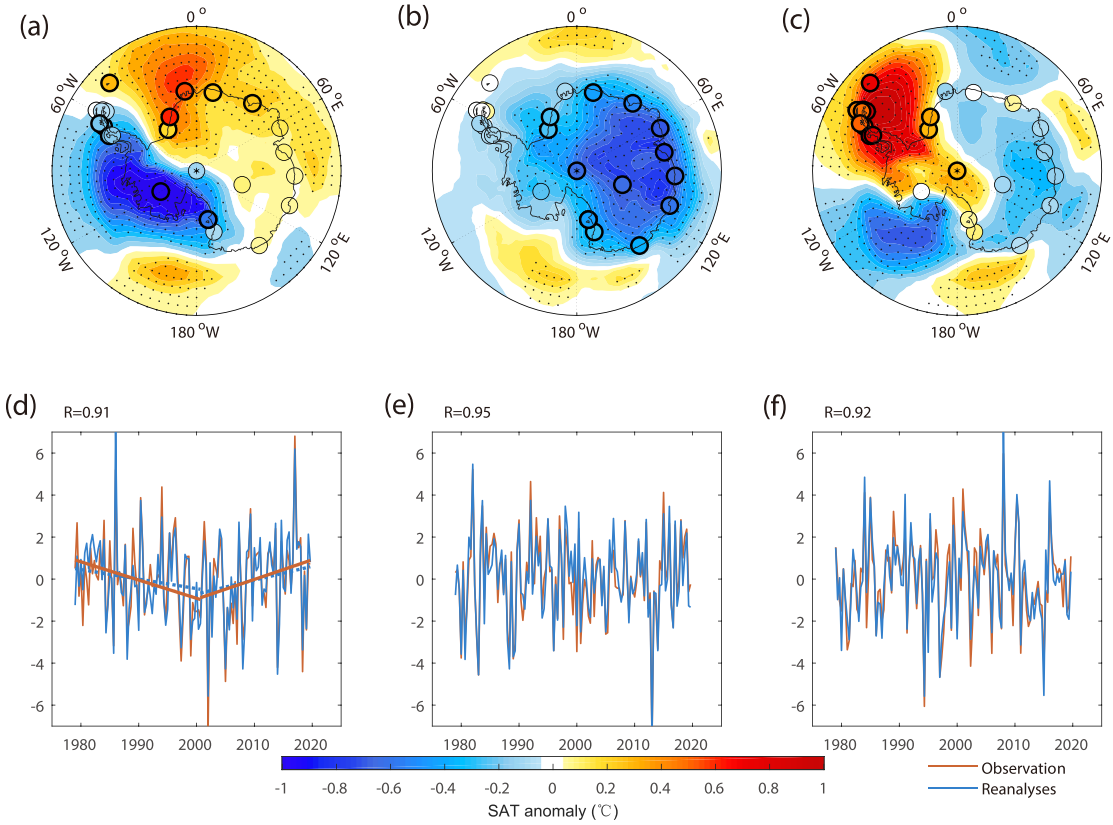

Figure 2. The first three major modes of the combined maximum covariance analysis (CMCA). Shown are results for austral spring from a set of 26 Antarctic station observations and 6 reanalysis datasets. (a) and (b) show the spatial pattern (a) and time series (b) of the CMCA Mode 1. The color shading represents the spatial patterns retrieved from 6 reanalysis datasets (ensemble mean for each mode), while the dots represent the signals of the 26 *in-situ* observations for each CMCA mode. The scatters show significant values at $p < 0.05$. The red and blue curves in (b) illustrate the CMCA time series of station observations (blue) and the combined reanalyses (red) for each mode, while the R values in the upper left corner of each panel indicate the correlation coefficient between these time series. (c)–(f) are same as (a) and (b), but for CMCA Mode 2 (c)–(d) and Mode 3 (e)–(f).

large-scale adjustments in thermal advection. In particular, during its positive phase (as shown in figure 3(a), predominantly post-2000), the deep low pressure center over the Antarctic Peninsula–Weddell Sea drives cold air advection from interior Antarctica to West Antarctica and warm advection from the Southern Ocean to Queen Maud Land. For the negative phase (predominantly pre-2000), the orientation of the above warm–cold advection is reversed (not shown), thus helping explain the switch of the seesaw SAT pattern in austral spring. The anomalous circulation pattern appears linked to the second PSA mode (PSA2); the correlation coefficient between the circulation pattern associated with the seesaw SAT mode (CMCA Mode 1) (i.e. figure 3(a)) and the PSA2 (figure 3(b)) reaches 0.91, and their temporal correlation coefficient is 0.6 (figure 3(c)).

The seesaw pattern shows strong signals along the coastal regions of the Queen Maud Land and the West Antarctic, as depicted in figures 2(a) and 3(a). To investigate the potential role of oceanic processes in these coastal signals, we conducted further analysis by calculating the sea ice concentration (SIC) and SST anomalies associated with the seesaw SAT mode in SON through linear regression (see supplementary figure 5). Our findings indicate that the high loadings across the coastal regions (figure 2(a)) are closely linked to the air–sea heat flux associated with the SIC and SST anomalies (see supplementary figure 5). Specifically, the positive phase of the seesaw mode (figure 2(a)) corresponds to a sea ice expansion over the Amundsen–Bellingshausen Sea and a sea ice retreat over the coastal East Antarctic (see supplementary figure 5(a)) caused by thermal advection and mechanical forcing [64, 65]. These sea ice anomalies further cool the West Antarctic and heat the East Antarctic by reducing/intensifying the heat flux from the ocean to the atmosphere [66, 67]. Additionally, the positive phase of the seesaw SAT mode is also closely associated with sea surface warming over the Atlantic sector of South Ocean and surface cooling over the Amundsen–Bellingshausen Sea (see supplementary figure 5(b)), which may contribute to the coastal warming/cooling over the East/West Antarctic by impacting on the sea ice anomalies [68] and air–sea heat flux. Therefore, the oceanic processes related to the SIC and SST anomalies play a crucial role in the high loading over the coastal regions of the seesaw SAT mode.

The circulation pattern associated with the Antarctic-continental mode (CMCA Mode 2) (see supplementary figure 6(a)) is dominated by

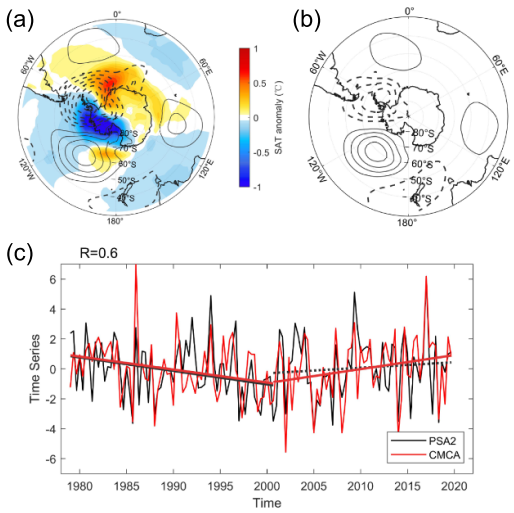

Figure 3. Sea level pressure (SLP) and surface air temperature (SAT) associated with CMCA Mode 1 and Pacific–South American pattern 2 (PSA2). (a) Spatial pattern of CMCA Mode 1 (color shadings) and regression map of sea level pressure (SLP, black contours) onto the normalized time series of Mode 1 during the period of 1979–2019. (b) Regression map of SLP against its normalized time series of PSA2. Solid contours show positive circulation anomalies, with dashed contours showing negative ones. Contour intervals are 0.5 hPa. (c) Time series of PSA2 (black curve) and CMCA Mode 1 (red curve). The solid (dashed) line shows the significant (insignificant) trend at $p < 0.05$. R values in the upper left corner of (c) indicate the correlation coefficient between the time series of CMCA Mode 1 and that of PSA2.

low-pressure encompassing the entire Antarctic continent, resembling the zonally symmetric SAM pattern with a spatial-pattern correlation reaching 0.85. The circulation associated with the Antarctic-dipole mode (CMCA Mode 3) (see supplementary figure 6(b)) shows a Rossby wave train pattern strongly resembling the first PSA mode (PSA1), with a correlation of about 0.64.

Recent studies [69, 70] indicated that the PSA2 is also associated with atmospheric internal variability including the ZW3 mode over the southern hemisphere. Correlation between the PSA2 and different atmospheric variables, including SAT, 500 hPa GPH, mean SLP, 500 hPa wind speed, and 10 m meridional wind speed, show clear ZW3 imprints in these fields (see supplementary figure 7). Composite anomalies over seven years with the largest (85th percentile) PSA2 years show that the positive phase of PSA2 is associated with a ∼30° (longitude) eastward shift of the ZW3 pattern (see supplementary figure 8), including a shift of the prominent Amundsen Sea Low (ASL) circulation mode eastward toward the Antarctic Peninsula and Weddell Sea, which here contributes to the deep pressure center over the Antarctic Peninsula–Weddell Sea after 2000.

4. Conclusion and discussion

Studies investigating Antarctic climate variability and trends are challenged by the limited observational data [3, 40]. Available *in-situ* observations are too sparse to represent variability over the entire Antarctic continent [7]. On the other hand, although we have many high-resolution gridded datasets, including satellite observations and reanalyses, the wide range of observational techniques, accuracies, and methods for combining observations and models necessarily lead to inconsistencies between different datasets [3, 40, 41]. Our application of the CMCA method extracts dominant modes of temperature variability in the station observations and six different reanalyses, one of which represents the coherent SAT mode featuring the Antarctic-seesaw pattern.

The dynamics of Antarctic climate change and its zonal-asymmetric feature is a fundamental issue in climate science [1, 71], especially given its broad implication for global sea level rise [10], global energy balance [11], and the global carbon cycle [12]. Recent studies indicated that the zonally asymmetric Antarctic SAT trends with East-cooling and West-warming during the second half of the 20th century were largely driven by the multi-decadal SST variability over the Pacific and the Atlantic Oceans. The SAM [60], the ASL [72, 73], and remote forcing from the tropical oceans [19, 22, 28] are each a part of the dynamics driving the observed Antarctic climate variability and change [22, 23, 28, 72–75], especially the dipole-like sea ice and SAT changes over the West Antarctic between the Ross Sea and Amundsen–Bellingshausen Seas.

Here we reveal a broader, continental-wide, seesaw SAT pattern between East and West Antarctica, which underwent a reversal around 2000 (figure 4). These reversed trends show strong warming over Queen Maud Land and inland East Antarctica and cooling over West Antarctica during 2000–2019. In contrast to previous studies that attributed the zonal asymmetry of the Antarctic SAT trend to the ASL [19, 20, 28, 76], we find that this continental-wide

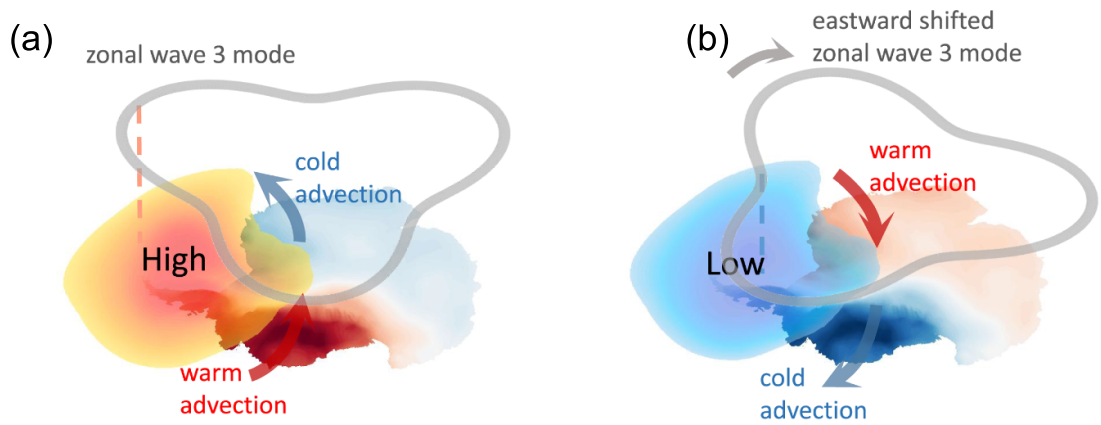

Figure 4. Schematic figure of the seesaw temperature pattern. The anomalous high (low) pressure center over the Antarctic Peninsula–Weddell Sea leads to warm (cold) advection to the West Antarctic region, with a cold (warm) advection to the East Antarctic region before (after) 2000, as shown in (a) and (b), leading to a surface air temperature seesaw pattern whose tendency switched before and after 2000. A reversal of this anomalous pressure center after 2000 is related to the eastward shift of the zonal wave number three mode.

seesaw SAT change is related to thermal advection caused by an anomalous circulation center over the Antarctic Peninsula–Weddell Sea region. Before 2000, there was an anomalous high-pressure center over the Peninsula–Weddell Sea region, leading to a warm air advection from lower latitudes to West Antarctica, and a cold air advection from the South Pole to Queen Maud Land (figure 4(a)). After 2000, an anomalous low-pressure center was present over the Peninsula–Weddell Sea region [5], reversing the patterns of thermal advection prior to 2000 (figure 4(b)). This anomalous circulation center is in part a result of forcing from the tropical Pacific, and in part an eastward shift of the ZW3 projected onto PSA2 variability, although the ultimate cause for the changes involving ZW3 and PSA2 requires further investigation, giving the dynamical complexity of the PSA2 [55, 69, 70, 77].

During the satellite era since 1979, the Antarctic has experienced a series of asymmetric climate changes, with the strongest changes typically appearing over the West Antarctic [2–4, 73]. The reversal of the Antarctic seesaw SAT trend pattern and the associated adjustment of the large-scale atmospheric circulation over the Antarctic we reported have broad implications for projecting long-term changes of the Antarctic sea-ice and land-ice [4–6, 9], in that these changes might not appear unidirectional and can be masked by the adjustment we documented. The Antarctic climate adjustment revealed by our study potentially has broad implications for the future projections of sea level rise, the energy budget of the earth system, and the global carbon cycle.

Data availability statement

All data that support the findings of this study are included within the article (and any supplementary files).

Acknowledgments

M X and X L is supported by the National Key Research and Development Program of China (2018YFA0605703), the Strategic Priority Research Program of Chinese Academy of Sciences Grant No. XDB42040106, and the National Natural Science Foundation of China (No. 42176243, No. 41976193 and Grant No. 41676190). K R C is supported by the Royal Society of New Zealand Marsden Fund Grant MFP-VUW2010. J T was supported by the UK Natural Environment Research Council (NERC) through the British Antarctic Survey research programme 'Polar Science for Planet Earth'. S E S was supported by the U.S. National Science Foundation (NSF) award PLR–1552226. J Z is supported by the Strategic Priority Research Program of Chinese Academy of Sciences Grant No. XDB42040100. W C is supported by the National Key Research and Development Program of China (2018YFA0605700), the Joint Research Centre for Southern Hemisphere Oceans Research (CSHOR) between the Qingdao National Laboratory for Marine Science and Technology (QNLM) and the Commonwealth Scientific and Industrial Research Organisation (CSIRO). The authors declare that they have no competing interests.

ORCID iDs

Jiang Zhu https://orcid.org/0000-0001-9846-8944
Xichen Li https://orcid.org/0000-0001-6325-6626

References

[1] Steig E J *et al* 2009 Warming of the Antarctic ice-sheet surface since the 1957 International Geophysical Year *Nature* **457** 459–62

[2] Bromwich D H et al 2013 Central West Antarctica among the most rapidly warming regions on Earth Nat. Geosci. 6 139–45
[3] Nicolas J P and Bromwich D H 2014 New reconstruction of Antarctic near-surface temperatures: multidecadal trends and reliability of global reanalyses J. Clim. 27 8070–93
[4] Shepherd A et al 2018 Mass balance of the Antarctic ice sheet from 1992 to 2017 Nature 558 219–22
[5] Simmonds I and Li M 2021 Trends and variability in polar sea ice, global atmospheric circulations, and baroclinicity Ann. New York Acad. Sci. 1504 167–86
[6] Parkinson C L and DiGirolamo N E 2021 Sea ice extents continue to set new records: Arctic, Antarctic, and global results Remote Sens. Environ. 267 112753
[7] Turner J et al 2019 Antarctic temperature variability and change from station data Int. J. Climatol. 40 2986–3007
[8] Pritchard H D et al 2012 Antarctic ice-sheet loss driven by basal melting of ice shelves Nature 484 502–5
[9] DeConto R M and Pollard D 2016 Contribution of Antarctica to past and future sea-level rise Nature 531 591–7
[10] Bamber J L, Westaway R M, Marzeion B and Wouters B 2018 The land ice contribution to sea level during the satellite era Environ. Res. Lett. 13 063008
[11] Kang S M, Frierson D M and Held I M 2009 The tropical response to extratropical thermal forcing in an idealized GCM: the importance of radiative feedbacks and convective parameterization J. Atmos. Sci. 66 2812–27
[12] Frölicher T L et al 2015 Dominance of the Southern Ocean in anthropogenic carbon and heat uptake in CMIP5 models J. Clim. 28 862–86
[13] Thompson D W and Solomon S 2002 Interpretation of recent Southern Hemisphere climate change Science 296 895–9
[14] Thompson D W et al 2011 Signatures of the Antarctic ozone hole in Southern Hemisphere surface climate change Nat. Geosci. 4 741–9
[15] Arblaster J M and Meehl G A 2006 Contributions of external forcings to southern annular mode trends J. Clim. 19 2896–905
[16] Turner J et al 2016 Absence of 21st century warming on Antarctic Peninsula consistent with natural variability Nature 535 411–5
[17] Zhang L, Delworth T L, Cooke W and Yang X 2019 Natural variability of Southern Ocean convection as a driver of observed climate trends Nat. Clim. Change 9 59–65
[18] Ding Q and Steig E J 2013 Temperature change on the Antarctic Peninsula linked to the tropical Pacific J. Clim. 26 7570–85
[19] Li X et al 2021 Tropical teleconnection impacts on Antarctic climate changes Nat. Rev. Earth Environ. 2 680–98
[20] Li X, Xie S-P, Gille S T and Yoo C 2016 Atlantic-induced pan-tropical climate change over the past three decades Nat. Clim. Change 6 275–9
[21] Fogt R L and Wovrosh A J 2015 The relative influence of tropical sea surface temperatures and radiative forcing on the Amundsen Sea Low J. Clim. 28 8540–55
[22] Li X, Holland D M, Gerber E P and Yoo C 2014 Impacts of the north and tropical Atlantic Ocean on the Antarctic Peninsula and sea ice Nature 505 538–42
[23] Simpkins G R, McGregor S, Taschetto A S, Ciasto L M and England M H 2014 Tropical connections to climatic change in the extratropical Southern Hemisphere: the role of Atlantic SST trends J. Clim. 27 4923–36
[24] Hsu P-C et al 2021 East Antarctic cooling induced by decadal changes in Madden-Julian oscillation during austral summer Sci. Adv. 7 eabf9903
[25] Mo K C and Paegle J N 2001 The Pacific–South American modes and their downstream effects Int. J. Climatol. A 21 1211–29
[26] Goyal R, Jucker M, Gupta A S and England M H 2022 A new zonal wave-3 index for the Southern Hemisphere J. Clim. 35 5137–49
[27] Irving D and Simmonds I 2015 A novel approach to diagnosing Southern Hemisphere planetary wave activity and its influence on regional climate variability J. Clim. 28 9041–57
[28] Ding Q, Steig E J, Battisti D S and Küttel M 2011 Winter warming in West Antarctica caused by central tropical Pacific warming Nat. Geosci. 4 398–403
[29] Fogt R L, Bromwich D H and Hines K M 2011 Understanding the SAM influence on the South Pacific ENSO teleconnection Clim. Dyn. 36 1555–76
[30] Schneider D P, Deser C and Okumura Y 2012 An assessment and interpretation of the observed warming of West Antarctica in the austral spring Clim. Dyn. 38 323–47
[31] Goosse H and Zunz V 2014 Decadal trends in the Antarctic sea ice extent ultimately controlled by ice-ocean feedback Cryosphere 8 453
[32] Hahn L C, Armour K C, Battisti D S, Donohoe A, Pauling A G and Bitz C M 2020 Antarctic elevation drives hemispheric asymmetry in polar lapse rate climatology and feedback Geophys. Res. Lett. 47 e2020GL088965
[33] Henley B J, Gergis J, Karoly D J, Power S, Kennedy J and Folland C K 2015 A tripole index for the interdecadal Pacific oscillation Clim. Dyn. 45 3077–90
[34] Meehl G A, Arblaster J M, Bitz C M, Chung C T and Teng H 2016 Antarctic sea-ice expansion between 2000 and 2014 driven by tropical Pacific decadal climate variability Nat. Geosci. 9 590–5
[35] Meehl G A, Hu A and Teng H 2016 Initialized decadal prediction for transition to positive phase of the interdecadal Pacific oscillation Nat. Commun. 7 1–7
[36] Clem K R, Lintner B R, Broccoli A J and Miller J R 2019 Role of the South Pacific convergence zone in West Antarctic decadal climate variability Geophys. Res. Lett. 46 6900–9
[37] Clem K R, Fogt R L, Turner J, Lintner B R, Marshall G J, Miller J R and Renwick J A 2020 Record warming at the South Pole during the past three decades Nat. Clim. Change 10 762–70
[38] Stammerjohn S E and Scambos T A 2020 Warming reaches the South Pole Nat. Clim. Change 10 710–1
[39] Wang Y, Wang M and Zhao J 2013 A comparison of MODIS LST retrievals with *in situ* observations from AWS over the Lambert Glacier Basin, East Antarctica Int. J. Geosci. 4 611–7
[40] Bracegirdle T J and Marshall G J 2012 The reliability of Antarctic tropospheric pressure and temperature in the latest global reanalyses J. Clim. 25 7138–46
[41] Wang Y, Zhou D, Bunde A and Havlin S 2016 Testing reanalysis data sets in Antarctica: trends, persistence properties, and trend significance J. Geophys. Res. Atmos. 121 12839–55
[42] Li J, Carlson B and Lacis A 2014 Application of spectral analysis techniques to the intercomparison of aerosol data–Part 4: synthesized analysis of multisensor satellite and ground-based AOD measurements using combined maximum covariance analysis Atmos. Meas. Technol. 7 2531–49
[43] Turner J, Colwell S R, Marshall G J, Lachlan-Cope T A, Carleton A M, Jones P D, Lagun V, Reid P A and Iagovkina S 2004 The SCAR READER project: toward a high-quality database of mean Antarctic meteorological observations J. Clim. 17 2890–8
[44] Saha S et al 2010 The NCEP climate forecast system reanalysis Bull. Am. Meteorol. Soc. 91 1015–58
[45] Saha S et al 2014 The NCEP climate forecast system version 2 J. Clim. 27 2185–208
[46] Kanamitsu M, Ebisuzaki W, Woollen J, Yang S-K, Hnilo J J, Fiorino M and Potter G L 2002 NCEP–DOE AMIP-II reanalysis (R-2) Bull. Am. Meteorol. Soc. 83 1631–44
[47] Gelaro R et al 2017 The modern-era retrospective analysis for research and applications, version 2 (MERRA-2) J. Clim. 30 5419–54
[48] Kobayashi S et al 2015 The JRA-55 reanalysis: general specifications and basic characteristics J. Meteorol. Soc. Japan Ser. II 93 5–48

[49] Dee D P et al 2011 The ERA-interim reanalysis: configuration and performance of the data assimilation system Q. J. R. Meteorol. Soc. 137 553–97
[50] Hersbach H et al 2020 The ERA5 global reanalysis Q. J. R. Meteorol. Soc. 146 1999–2049
[51] Gossart A, Helsen S, Lenaerts J T M, Broucke S V, van Lipzig N P M and Souverijns N 2019 An evaluation of surface climatology in state-of-the-art reanalyses over the Antarctic ice sheet J. Clim. 32 6899–915
[52] Zhu J, Xie A, Qin X, Wang Y, Xu B and Wang Y 2021 An assessment of ERA5 reanalysis for Antarctic near-surface air temperature Atmosphere 12 217
[53] Rayner N et al 2003 Global analyses of sea surface temperature, sea ice, and night marine air temperature since the late nineteenth century J. Geophys. Res. Atmos. 108 4407
[54] Xin M, Li X, Zhu J, Song C, Zhou Y, Wang W and Hou Y 2023 Characteristic features of the Antarctic surface air temperature with different reanalyses and in situ observations and their uncertainties Atmosphere 14 464
[55] Mo K C 2000 Relationships between low-frequency variability in the Southern Hemisphere and sea surface temperature anomalies J. Clim. 13 3599–610
[56] Sen P K 1968 Estimates of the regression coefficient based on Kendall's tau J. Am. Stat. Assoc. 63 1379–89
[57] Kendall M G 1975 Rank Correlation Methods (New York: Oxford University Press)
[58] Alin A, Beyaztas U and Martin M A 2019 Robust change point detection for linear regression models Stat. Interface. 12 203–13
[59] Yan Z W, Ye D Z and Wang C 1992 Climatic jumps in the flood/drought historical chronology of central China Clim. Dyn. 6 153–60
[60] Marshall G J 2003 Trends in the Southern Annular Mode from observations and reanalyses J. Clim. 16 4134–43
[61] Li S, Cai W and Wu L 2021 Weakened Antarctic Dipole under global warming in CMIP6 models Geophys. Res. Lett. 48 e2021GL094863
[62] Yuan X and Martinson D G 2001 The Antarctic dipole and its predictability Geophys. Res. Lett. 28 3609–12
[63] Li S, Cai W and Wu L 2020 Attenuated interannual variability of austral winter Antarctic sea ice over recent decades Geophys. Res. Lett. 47 e2020GL090590
[64] Holland P R and Kwok R 2012 Wind-driven trends in Antarctic sea-ice drift Nat. Geosci. 5 872–5
[65] Lefebvre W and Goosse H 2005 Influence of the Southern Annular Mode on the sea ice-ocean system: the role of the thermal and mechanical forcing Ocean Sci. Discuss. 2 299–329
[66] DeConto R, Pollard D and Harwood D 2007 Sea ice feedback and Cenozoic evolution of Antarctic climate and ice sheets Paleoceanography 22 PA3214
[67] Sandven S, Johannessen O M and Kloster K 2006 Sea ice monitoring by remote sensing Encyclopedia of Analytical Chemistry pp 241–83
[68] Kumar A, Yadav J and Mohan R 2021 Seasonal sea-ice variability and its trend in the Weddell Sea sector of West Antarctica Environ. Res. Lett. 16 024046
[69] Irving D and Simmonds I 2016 A new method for identifying the Pacific–South American pattern and its influence on regional climate variability J. Clim. 29 6109–25
[70] O'Kane T J, Monselesan D P and Risbey J S 2017 A multiscale reexamination of the Pacific–South American pattern Mon. Weather Rev. 145 379–402
[71] Meehl G A, Arblaster J M, Chung C T Y, Holland M M, DuVivier A, Thompson L, Yang D and Bitz C M 2019 Sustained ocean changes contributed to sudden Antarctic sea ice retreat in late 2016 Nat. Commun. 10 1–9
[72] Raphael M, Marshall G J, Turner J, Fogt R L, Schneider D, Dixon D A, Hosking J S, Jones J M and Hobbs W R 2016 The Amundsen Sea Low: variability, change, and impact on Antarctic climate Bull. Am. Meteorol. Soc. 97 111–21
[73] Turner J, Phillips T, Hosking J S, Marshall G J and Orr A 2013 The Amundsen Sea low Int. J. Climatol. 33 1818–29
[74] Ciasto L M, Simpkins G R and England M H 2015 Teleconnections between tropical Pacific SST anomalies and extratropical Southern Hemisphere climate J. Clim. 28 56–65
[75] Sato K, Inoue J, Simmonds I and Rudeva I 2021 Antarctic Peninsula warm winters influenced by Tasman Sea temperatures Nat. Commun. 12 1497
[76] Jun S-Y, Kim J-H, Choi J, Kim S-J, Kim B-M and An S-I 2020 The internal origin of the west-east asymmetry of Antarctic climate change Sci. Adv. 6 eaaz1490
[77] Rodrigues R R, Campos E J and Haarsma R 2015 The impact of ENSO on the South Atlantic subtropical dipole mode J. Clim. 28 2691–705